J. Math. Biol. (1991) 29: 629–651

Journal of
Mathematical
Biology

An eikonal-curvature equation for action potential propagation in myocardium*

James P. Keener
Department of Mathematics, University of Utah, Salt Lake City, Utah 84112, USA

Received July 5, 1990; received in revised form October 15, 1990

Abstract. We derive an "eikonal-curvature" equation to describe the propagation of action potential wavefronts in myocardium. This equation is used to study the effects of fiber orientation on propagation in the myocardial wall. There are significant computational advantages to the use of an eikonal-curvature equation over a full ionic model of action potential spread. With this model, it is shown that the experimentally observed misalignment of spreading action potential "ellipses" from fiber orientation in level myocardial surfaces is adequately explained by the rotation of fiber orientation through the myocardial wall. Additionally, it is shown that apparently high propagation velocities on the epicardial and endocardial surfaces are the result of propagation into the midwall region and acceleration along midwall fibers before reemergence at an outer surface at a time preceding what could be accomplished with propagation along the surface alone.

Key words: Action potential propagation – Anisotropy eikonal-curvature equation

Introduction

About once each second, a deflection of the transmembrane potential, called an action potential, propagates across your myocardium to initiate the pumping action necessary to sustain life. An action potential travels at about half a meter per second, has a duration of about 0.3 seconds, and consists of a rapidly rising upstroke, a flat plateau, and a downstroke. Mathematical descriptions of action potentials are usually provided by empirically derived systems of differential equations of Hodgkin–Huxley type [3, 10, 15, 22, 24, 39], describing ionic currents that accompany each action potential. The drawbacks of these models are numerous, since the descriptions of single cells are quite complex, and not quantitatively accurate during certain phases of the action potential, and to study the behavior of propagating action potentials with these models for realistic tissue structure is at best an enormous undertaking.

An alternate approach is to study simplified model equations that capture the

* Research was supported in part by NSF Grant DMS-8801446

important features, but do not rely in explicit detail on the specific nature of an ionic model. To this end, an eikonal equation approach suggests itself. That is, since an action potential has a rapidly rising leading edge that occupies only a few cell lengths [7], perhaps it is possible to idealize the location of this front as a moving surface in the myocardial wall and to derive an equation for its motion that holds regardless of the details of one's favorite ionic model. Certainly, in mapping studies of action potential propagation, experimentalists routinely use the idealization that an action potential upstroke is, for all practical purposes, a localized moving front. Perhaps theorists would do well to follow suit.

If a propagating action potential can be viewed as a localized moving surface, we would like the equation of motion to specify the normal velocity of the surface as a function of its shape and local properties of the medium. We might guess that an "eikonal-curvature" equation [19, 25] would suffice, since it applies so nicely to other excitable media. An eikonal-curvature equation has been used successfully for Belousov–Zhabotinsky reagent [37, 12], and for two dimensional layers of myocardium [7], as well as in other nonbiological contexts [4, 13]. However, three dimensional myocardium is different from these other media, since propagation is faster in the direction of the cell's long axis than transverse to the cell. Furthermore, the cell axis rotates through about 120 degrees counterclockwise from epicardium to endocardium [34, 23]. In thin layers of myocardial tissue, we can account for the anisotropy by a simple linear change of spatial scale applied to the eikonal-curvature equation, but for fully three dimensional tissue, this easy remedy does not work.

The purpose of this paper is twofold. First, we wish to demonstrate the superiority of an eikonal-curvature equation approach over the more traditional approach of directly simulating an ionic model. To simulate an ionic model, since the action potential upstroke is fast and localized in space, it is typical to use a finely resolved spatial grid, on the order of one grid point per cell, but not less [2, 6, 8, 9, 16, 17, 18, 28]. If fewer grid points are used, then artifactual propagation block results since too much resistance is clumped together into one grid point [18]. With a finely resolved grid, study of a large tissue patch is impossible, even with present day supercomputers. For example, in Section 6, we present results for a 5 cm $\times$ 5 cm $\times$ 1 cm piece of myocardial wall. To simulate an ionic model for this domain using one grid point per cell would require roughly 10^9 grid points. In comparison, the simulation shown here used a mere 2×10^5 grid points. Furthermore, if a simple explicit numerical integration scheme is used to simulate an ionic model, the time step must be restricted to be on the order of the space step squared, leading to very long integration times. Of course, one can use more sophisticated implicit schemes or adaptive grid techniques that place a finely discretize grid only in the region of large spatial and temporal gradients. However, the claim of this paper is that if one wants to know where an action potential wavefront is located, and is willing to overlook the details of the upstroke, then savings of many orders of magnitude can be effected.

Second, we wish to study the effect of fiber orientation on action potential propagation. Since propagation is fastest along fibers it is commonly held that an action potential spreads with elliptical shape whose major axis is in the fiber direction. This is apparently correct in thin layers of myocardium, but for intact myocardial wall, recent measurements [14] have shown that, while the spread is roughly elliptical in shape, the major axis of spread is definitely not along the fiber axis. In this study, we show that changing fiber orientation accounts for these experimental findings.

The outline of this paper is as follows: In the next section we will describe our notation and the basic equations of action potential behavior. In Section 3 we will study the behavior of propagation in a one dimensional cable. The purpose of this one dimensional study is to understand the effect of tissue inhomogeneity on propagation, and to gain confidence in the approximate derivation that will be used later. In Section 4, we derive the eikonal-curvature equation appropriate for fully general (anisotropic, inhomogeneous) three dimensional tissue. In Section 5, we discuss some two dimensional solutions of this equation. Finally, in Section 6, we discuss the behavior of solutions for propagation in three dimensional myocardial tissue.

2 The model equations

An action potential is observable as a deflection of the transmembrane potential, and we determine the transmembrane potential by keeping track of all of the currents. It is usual to view the cell's membrane as a leaky capacitor, so a simple conservation statement is

$$I = C_m \frac{\partial \phi}{\partial t} - I_m, \tag{2.1}$$

where I represents the total outward transmembrane current per unit area of membrane, I_m is the total inward ionic current per unit area of membrane, C_m is the per unit area capacitance of the membrane, and ϕ is the transmembrane potential calculated as the difference between the internal and external potentials, $\phi = \phi_i - \phi_e$. The membrane resistance R_m is defined as the inverse slope of the transmembrane current for potentials near the resting potential, that is, $R_m I_m = -\delta\phi$, where $\delta\phi$ is the deviation of the transmembrane potential from its polarized resting state. We shall always measure time on a time scale in which $R_m C_m = 1$. Typical parameter values are $C_m = 0.8\text{–}1.0\ \mu\text{F cm}^{-2}$, and $R_m = 5.0\text{–}9.0 \times 10^3\ \Omega\ \text{cm}^2$ [38], yielding a typical time unit on the order of 4.0–9.0 msec. A list of the most commonly used symbols is given in Table 1.

We view the intracellular space (subscript i) and extracellular space (subscript e) as two comingled continuous domains (a bidomain model [27]), each

Table 1. Commonly used symbols

Symbol	Meaning	Dimensions
C_m	membrane capacitance per unit area	$\mu\text{F cm}^{-2}$
R_m	membrane resistance	$\Omega\ \text{cm}^2$
ϕ	transmembrane potential	mvolts
ϕ_e	extracellular potential	mvolts
ϕ_i	intracellular potential	mvolts
S	cell surface area	cm^2
V	cell volume	cm^3
$D_j, j = 1, 2, 3$	intracellular coupling strength	cm^2
$d_j, j = 1, 2, 3$	extracellular coupling strength	cm^2
d_i	intracellular coupling strength for 1-d cable	cm^2
d_e	extracellular coupling strength for 1-d cable	cm^2
L	thickness of myocardial wall	cm

taking a fixed fraction of the total available volume. Accordingly, the current flow between these two domains must equal the divergence of the currents within each region, i.e.,

$$\frac{S}{V} I = \operatorname{div}(i_e) = -\operatorname{div}(i_i), \tag{2.2}$$

where S/V is the ratio of membrane surface area to volume of tissue (on the order of 10^3 cm^{-1} for myocardium), and i_i and i_e are intracellular and extracellular current densities (i.e., current per unit cross-sectional area). Finally, we relate the currents to the potentials through Ohm's law. Because the medium is anisotropic, the easiest coordinate system in which to write Ohm's law is the natural coordinate system of the cells, i.e. taking X_1 in the direction of the cell axis, X_2 and X_3 orthogonal to the cell axis. Then we can write

$$\frac{R_m V}{S} i_i = -\sum_{j=1}^{3} D_j \frac{\partial \phi_i}{\partial X_j} \boldsymbol{I}_j, \qquad \frac{R_m V}{S} i_e = -\sum_{j=1}^{3} d_j \frac{\partial \phi_e}{\partial X_j} \boldsymbol{I}_j, \tag{2.3}$$

where d_j and D_j are the extracellular and intracellular coupling strengths, measured in units of cm^2, and $\boldsymbol{I}_j$ is the unit vector in the jth direction. The coupling coefficients D_j and d_j are of the order of magnitude of a space constant squared, or about 1 mm^2 in the fiber direction. More precisely, in any of the coordinate directions, if D_j and d_j are constants, the space constant for that direction Λ_j satisfies $1/\Lambda_j^2 = 1/D_j + 1/d_j$. If the medium is inhomogeneous, the coefficients d_j and D_j depend on position.

Since the cell axis direction varies through the thickness of the myocardium, the X_j coordinates are not the correct coordinates to use. Instead we use a fixed orthogonal coordinate system, say x_j, with $x_3 = X_3$ the direction through the myocardial thickness. We assume that fibers are all parallel to the epicardial plane. In terms of a fixed extrinsic coordinate system we find,

$$\begin{aligned}
\text{a)} \quad -\frac{R_m V}{S} i_e = &\left((d_1 \cos^2\theta + d_2 \sin^2\theta) \frac{\partial \phi_e}{\partial x_1} + (d_1 - d_2) \sin\theta \cos\theta \frac{\partial \phi_e}{\partial x_2} \right) \boldsymbol{i}_1 \\
&+ \left((d_2 \cos^2\theta + d_1 \sin^2\theta) \frac{\partial \phi_e}{\partial x_2} + (d_1 - d_2) \sin\theta \cos\theta \frac{\partial \phi_e}{\partial x_1} \right) \boldsymbol{i}_2 \\
&+ d_3 \frac{\partial \phi_e}{\partial x_3} \boldsymbol{i}_3,
\end{aligned} \tag{2.4}$$

$$\begin{aligned}
\text{b)} \quad -\frac{R_m V}{S} i_i = &\left((D_1 \cos^2\theta + D_2 \sin^2\theta) \frac{\partial \phi_i}{\partial x_1} + (D_1 - D_2) \sin\theta \cos\theta \frac{\partial \phi_i}{\partial x_2} \right) \boldsymbol{i}_1 \\
&+ \left((D_2 \cos^2\theta + D_1 \sin^2\theta) \frac{\partial \phi_i}{\partial x_2} + (D_1 - D_2) \sin\theta \cos\theta \frac{\partial \phi_i}{\partial x_1} \right) \boldsymbol{i}_2 \\
&+ D_3 \frac{\partial \phi_i}{\partial x_3} \boldsymbol{i}_3,
\end{aligned}$$

where $\theta = \theta(x_3)$ is the angle the long axis of the cell makes with the x_1 axis in some layer of myocardium with x_3 fixed, and $\boldsymbol{i}_j$, $j = 1, 2, 3$ are the unit vectors in

the fixed extrinsic coordinate system. Combining (2.2) and (2.4) we find that the transmembrane current is given by

$$-R_m I = \frac{\partial}{\partial x_1}\left((d_1 \cos^2\theta + d_2 \sin^2\theta)\frac{\partial \phi_e}{\partial x_1} + (d_1 - d_2)\sin\theta\cos\theta\frac{\partial \phi_e}{\partial x_2}\right)$$
$$+\frac{\partial}{\partial x_2}\left((d_2 \cos^2\theta + d_1 \sin^2\theta)\frac{\partial \phi_e}{\partial x_2} + (d_1 - d_2)\sin\theta\cos\theta\frac{\partial \phi_e}{\partial x_1}\right)$$
$$+\frac{\partial}{\partial x_3}\left(d_3\frac{\partial \phi_e}{\partial x_3}\right), \tag{2.5}$$

and

$$R_m I = \frac{\partial}{\partial x_1}\left((D_1 \cos^2\theta + D_2 \sin^2\theta)\frac{\partial \phi_i}{\partial x_1} + (D_1 - D_2)\sin\theta\cos\theta\frac{\partial \phi_i}{\partial x_2}\right)$$
$$+\frac{\partial}{\partial x_2}\left((D_2 \cos^2\theta + D_1 \sin^2\theta)\frac{\partial \phi_i}{\partial x_2} + (D_1 - D_2)\sin\theta\cos\theta\frac{\partial \phi_i}{\partial x_1}\right)$$
$$+\frac{\partial}{\partial x_3}\left(D_3\frac{\partial \phi_i}{\partial x_3}\right). \tag{2.6}$$

A complete description of the potentials requires additional equations to determine the time dependent behavior of ionic currents, but these are assumed to be transmembrane currents only, and therefore add no derivatives with respect to the spatial coordinates. Propagation of action potentials is controlled by the fast ionic currents, namely the (instantaneous) rectifier potassium current i_{k1}, and the fast sodium current. Other currents, such as potassium and calcium, are important only later during the action potential and determine action potential duration and recovery of excitability. A good approximation for I_m during the action potential upstroke is found by setting the sodium activation m (in the notation of Hodgkin and Huxley [15]) equal to its voltage dependent equilibrium $m_\infty(v)$, and to hold all other activation and inactivation variables fixed at their resting potential values. For all ionic models, the result of this simplification is a function I_m depending only on the transmembrane potential ϕ, having three zeros, say $\Phi_0 < \Phi_1 < \Phi_2$, with $I_m(\phi) < 0$ on the interval $\Phi_0 < \phi < \Phi_1$ and $I_m(\phi) > 0$ on the interval $\Phi_1 < \phi < \Phi_2$. Since the slope of $I_m(\phi)$ at Φ_0 is $-1/R_m$, we define a scaled current function $f(\phi) = R_m I_m(\phi)$. The function $f(\phi)$ has units of volts.

Our goal is to study propagation of action potentials as governed by the conservation equation (2.1) and the constitutive equations (2.5) and (2.6) assuming that the fiber orientation is a function of distance through the wall x_3, i.e., $\theta = \theta(x_3)$.

Hidden inside the equations (2.1), (2.5), (2.6) is a simple equation trying to get out. The simple equation is

$$\Phi'' + c_0\Phi' + f(\Phi) = 0, \tag{2.7}$$

where number c_0 is a dimensionless number. A goal of this paper is to approximate the solution of the full governing equations (2.1), (2.5) and (2.6) using the solution of equation (2.7). Thus, throughout this paper we will use the fact [1, 11] that there is a unique positive value of the parameter c_0 for which a monotone decreasing

solution $\Phi(x)$ of (2.7) exists with $\lim_{x\to\infty}\Phi(x)=\Phi_0$, $\lim_{x\to-\infty}\Phi(x)=\Phi_2$. The function $\Phi(x)$ represents a traveling action potential front, providing a transition between the resting potential Φ_0 and the "excited" state Φ_2. The number c_0 is a measure of the excitability of the medium, depending solely on the details of the function f, and is smaller for a relatively unrecovered medium than for a well recovered medium. The number c_0 can be measured experimentally or calculated from one's favorite membrane model.

3 One dimensional propagation

In this section we study propagation in a one dimensional cable. The purpose of this discussion is to understand the effects of inhomogeneity on the speed of propagation and shape of the action potential front, and also to develop a mathematical method that will generalize to the more difficult three dimensional problem in the next section. In one spatial dimension the equations (2.1), (2.5), and (2.6) reduce to

$$\begin{aligned}\frac{\partial\phi}{\partial t}&=\frac{\partial}{\partial x}\left(d_i\frac{\partial\phi_i}{\partial x}\right)+f(\phi),\\ \frac{\partial\phi}{\partial t}&=-\frac{\partial}{\partial x}\left(d_e\frac{\partial\phi_e}{\partial x}\right)+f(\phi),\end{aligned}\tag{3.1}$$

where the functions d_i and d_e are the intracellular and extracellular coupling coefficients, respectively, assumed to be functions of x, measured in units of cm^2. Nontrivial x dependence is used to account for local variations in cable thickness or longitudinal resistance due to gap junctions, for example. Recall that time is always measured on the time scale in which $R_mC_m=1$. Subtracting the two equations (3.1) we find that

$$\frac{\partial}{\partial x}\left(d_i\frac{\partial\phi_i}{\partial x}+d_e\frac{\partial\phi_e}{\partial x}\right)=0.\tag{3.2}$$

Supposing there to be no net axial current at infinity, we take

$$d_i\frac{\partial\phi_i}{\partial x}+d_e\frac{\partial\phi_e}{\partial x}=0,$$

which when coupled with $\phi=\phi_i-\phi_e$, implies that

$$\frac{\partial\phi_e}{\partial x}=\frac{d_i}{d_i+d_e}\phi_x,\qquad \frac{\partial\phi_i}{\partial x}=\frac{-d_e}{d_i+d_e}\phi_x.\tag{3.3}$$

Substituting (3.3) into (3.1) we find the equation governing the evolution of transmembrane potential ϕ is

$$\frac{\partial\phi}{\partial t}=\frac{\partial}{\partial x}\left(d\frac{\partial\phi}{\partial x}\right)+f(\phi),\tag{3.4}$$

where $1/d=1/d_e+1/d_i$.

In the special case that d is a constant (i.e., the medium is uniform) we find an exact traveling wave solution

$$\phi(x,t)=\Phi\left(\frac{x}{\sqrt{d}}-c_0t\right),\tag{3.5}$$

where $\Phi(x)$ is the known solution of the equation (2.7). In other words, there is a traveling wave solution for the action potential front traveling with speed $c = c_0\sqrt{d}$. The spatial scale of this traveling wave solution is governed by the scalar d. That is, if d is small, then the action potential front is sharp, localized to have a large gradient over a spatial domain of the order of the size of $\sqrt{d}$. The number $\sqrt{d}$ is the space constant for myocardium [21], which is about 0.09 cm in the fiber direction and about 0.03 cm transverse to fibers, although the action potential front is somewhat more localized than this.

To study the effects of inhomogeneity, we seek propagating solutions of (3.4) assuming that d is a slowly varying function of x. That is, d does not vary much over the length scale of a typical action potential front, namely a length on the order of a space constant $\sqrt{d}$. Said another way, we suppose that d is a function of εx, where $\varepsilon\sqrt{d}$ is everywhere small. It is also possible to include other effects of tissue inhomogeneity by assuming that f is a slowly varying function of x, but we shall not include this effect here.

We cannot solve this problem exactly, so we use an approximate approach. An approximate solution of the problem (3.4) can be found using a standard multiscale perturbation argument [20]. The idea is to assume (i.e., pretend) that there are four independent variables, two fast variables and two slow variables, rather than just two independent variables. We let $\tau = \varepsilon t$, $\sigma = \varepsilon x$ be the slow variables, and y and $\xi = y - c_0 t$ be the fast variables, where $dy/dx = g(\sigma)$ is yet to be determined. The variable y will be used to remove slowly varying spatial inhomogeneity, and is suggested by the study of adiabatic invariance [5, 20]. It follows from the chain rule that

$$\begin{aligned} \frac{\partial}{\partial t} &= -c\frac{\partial}{\partial \xi} + \varepsilon\frac{\partial}{\partial \tau}, \\ \frac{\partial}{\partial x} &= g(\sigma)\frac{\partial}{\partial \xi} + \varepsilon\frac{\partial}{\partial \sigma}, \end{aligned} \tag{3.6}$$

so that

$$\frac{\partial}{\partial x}\left(d(\varepsilon x)\frac{\partial \phi}{\partial x}\right) = g(\sigma)^2 d(\sigma)\phi_{\xi\xi} + 2\varepsilon g(\sigma)d(\sigma)\phi_{\xi\sigma} + \varepsilon(d(\sigma)g(\sigma))_\sigma \phi_\xi + \varepsilon^2(d(\sigma)\phi_\sigma)_\sigma. \tag{3.7}$$

We seek an asymptotic expansion for ϕ by assuming that $\phi = \phi^0 + \varepsilon u$. Then, to leading order in ε, we must satisfy the equation

$$g^2 d\phi^0_{\xi\xi} + c_0\phi^0_\xi + f(\phi^0) = 0. \tag{3.8}$$

A key step is to pick $g(\sigma)$ so that the leading order solution is independent of σ. This we accomplish by taking

$$g^2 = \frac{1}{d}, \tag{3.9}$$

and then it follows that

$$\phi^0 = \Phi(\xi + \theta(\sigma, \tau)), \tag{3.10}$$

where $\Phi(x)$ is the known solution of (2.7).

The phase shift θ is determined from the next order equation

$$u_{\xi\xi} + c_0 u_\xi + f'(\phi^0)u = \phi^0_\tau - \frac{2}{g}\phi^0_{\sigma\xi} - \left(\frac{1}{g}\right)_\sigma \phi^0_\xi. \tag{3.11}$$

The important observation is that equation (3.11) has a bounded solution if and only if the right hand side of the equation is orthogonal to the function $\exp(c_0\xi)\phi_\xi^0$. This follows from the Fredholm Alternative theorem [20] and the fact that the differential equation $u_{\xi\xi} + c_0 u_\xi + f'(\phi^0)u = 0$ has a null space spanned by $u = \phi_\xi^0$ while the adjoint equation $w_{\xi\xi} - c_0 w_\xi + f'(\phi^0)w = 0$ has a null space spanned by $\exp(c_0\xi)\phi_\xi^0$. Therefore, after multiplying (3.11) by $\exp(c_0\xi)\phi_\xi^0$ and integrating by parts, we find

$$\int_{-\infty}^{\infty} \left(\phi_\tau^0 - \frac{2}{g}\phi_{\sigma\xi}^0 - \left(\frac{1}{g}\right)_\sigma \phi_\xi^0\right) \exp(c_0\xi)\phi_\xi^0 \, d\xi = 0. \tag{3.12}$$

On substituting the form of the solution (3.10) into (3.12), we find the differential equation for the phase θ,

$$\theta_\tau = -\frac{c_0}{g}\theta_\sigma + \left(\frac{1}{g}\right)_\sigma. \tag{3.13}$$

We take

$$c_0\theta = -\ln(g(\sigma)) \tag{3.14}$$

as the bounded solution of (3.13). The approximate solution of the full problem becomes, to leading order in ε,

$$\phi(x, t) = \Phi\left(\int_0^x g(\varepsilon y)\, dy - \frac{1}{c_0}\ln(g(\varepsilon x)) - c_0 t\right) + O(\varepsilon), \tag{3.15}$$

where $g(\sigma) = 1/\sqrt{d(\sigma)}$.

There are two interesting observations to make about this solution representation. Certainly, the function (3.15) is not a translation invariant traveling wave solution. At each point in space, the time history of the action potential is the same, but the speed of propagation and the spatial shape of the action potential front have nontrivial dependence on space.

The local speed of propagation is defined as the speed of a space-time curve along which the argument of Φ in (3.15) remains constant. It is easy to see that this speed is

$$\frac{dx}{dt} = \frac{c_0}{g - \frac{1}{c_0}\frac{d}{dx}\ln(g(\varepsilon x))} = \frac{c_0\sqrt{d}}{1 + \frac{d_x}{2c_0\sqrt{d}}}. \tag{3.16}$$

Here we see an interesting effect. The local speed of propagation increases when coupling d increases, as we would expect. The value $c_0\sqrt{d}$ is the speed predicted by the solution (3.5) when the cable is uniform. However, the speed is also affected by the derivative of d in the opposite direction. That is, if d is increasing there is an additional speed decrement. This makes physical sense, since the load is higher and propagation slower in a cable in which resistance is decreasing, than in a uniform cable. Thus, the derivative term in (3.16) acts like an inertial term which takes into account the derivatives of the local cable properties.

The relative effect of the derivative term in (3.16) is governed by the excitability of the medium. In a highly excitable medium, c_0 is large and the relative effect of the derivative term is small, so that the result for a uniform cable is nearly correct. For a less excitable medium, with c_0 quite small, the relative effect of the derivative term is large. For small enough c_0, the approximation (3.16) is obviously wrong, since a zero or negative denominator is not

permitted. However, this does suggest that there may be some combinations of coupling strength and excitability that preclude action potential propagation, and indeed this is known to be the case [21].

The next interesting effect is on the spatial configuration of the wave shape. Because the curves of constant argument in (3.15) are not straight, there are regions where they are "bunched together" and there are other regions where they are "spread apart". This leads to a spatial distribution for the action potential front that is relatively flat in regions of low resistance and relatively steep in regions of high resistance. There is experimental evidence for the validity of these expressions, since propagation, especially in relatively unrecovered tissue, or tissue where gap junction function is known to be impaired, is observed to be "saltatory", appearing to propagate rapidly through individual cells, and slowly through gap junctions [32, 31]. Numerical simulations have also shown this discontinuous appearance [29].

The preceding arguments used a standard multi-scale argument to determine the velocity of the action potential front as it moves along a nonuniform excitable cable. There is another way to derive an equivalent result that is easier to apply in the higher dimensional case. The idea is to find a new coordinate system in which the equation (3.5) has the form of the equation (2.7). To that end, we introduce a general moving coordinate system $x = X(\xi, \tau)$, $t = \tau$, taking $X_\xi = \sqrt{d(X)}$. It follows from the chain rule that

$$\phi_\tau = \phi_{\xi\xi} + \left(\frac{X_\tau}{\sqrt{d(X)}} + (\sqrt{d(X)})_x \right) \phi_\xi + f(\phi). \tag{3.17}$$

We find a steady solution of the equation (3.17) by setting $\phi_\tau = 0$, and by requiring that

$$X_\tau = c_0 \sqrt{d(X)} - \tfrac{1}{2}(d(X))_x. \tag{3.18}$$

It is too much to expect that both (3.18) and $X_\xi = \sqrt{d(X)}$ can be satisfied everywhere. However, if the medium is slowly varying in space, we solve these locally. That is, we require that (3.18) be satisfied in the region where the gradient ϕ_x is largest, i.e., at the center of the action potential front, and then equation (3.18) becomes an equation for the velocity of the front.

The equation (3.18) for the motion of the front is a one dimensional eikonal equation, as it specifies the velocity of the front as a function of its position. It is easy to see that (3.18) agrees with (3.16) when the medium is slowly varying in space.

4 Three dimensional eikonal-curvature equation

Our goal in this section is to use arguments similar to those at the end of the preceding section to find an equation governing the motion of a sharp action potential front in a general three dimensional slowly varying medium. Our approach will be to change coordinates to a general moving coordinate system, and then allow the coordinate system to move so that the profile of the action potential front is governed approximately by (2.7).

It simplifies our calculations substantially to assume that coupling in the extracellular medium is infinitely strong. While this is incorrect for myocardium,

it has little effect on our results. If the extracellular medium is assumed to be isopotential, we can take $\phi_e = 0$, $\phi_i = \phi$. We take as our governing equations

$$\frac{\partial \phi}{\partial t} = \frac{\partial}{\partial x_i}\left(d_{ij}\frac{\partial \phi}{\partial x_j}\right) + f, \tag{4.1}$$

where here and throughout the rest of this paper, the summation convention is assumed (sum over doubly repeated indices). We assume general coupling coefficients d_{ij} for the intracellular domain. Later we shall use the specific choices of coupling indicated by (2.4a). We take the coupling matrix to be symmetric, $d_{ij} = d_{ji}$.

We introduce a general moving coordinate system $x = X(\xi, \tau)$, $t = \tau$. According to the chain rule,

$$\frac{\partial}{\partial \xi_i} = \frac{\partial X_j}{\partial \xi_i}\frac{\partial}{\partial x_j} \quad \text{and} \quad \frac{\partial}{\partial \tau} = \frac{\partial}{\partial t} + \frac{\partial X_j}{\partial \tau}\frac{\partial}{\partial x_j}.$$

It follows that

$$\frac{\partial}{\partial x_i} = \alpha_{ij}\frac{\partial}{\partial \xi_j} \quad \text{and} \quad \frac{\partial}{\partial t} = \frac{\partial}{\partial \tau} - \frac{\partial X_j}{\partial \tau}\alpha_{jk}\frac{\partial}{\partial \xi_k}, \tag{4.2}$$

where the matrix with entries α_{ij} is the inverse of the matrix with entries $\partial X_j/\partial \xi_i$.

We identify the variable ξ_1 as the coordinate normal to level surfaces of action potential activity, so ξ_2 and ξ_3 are the coordinates of the moving level surfaces. Then, we define the tangent vectors $r_i = \partial X/\partial \xi_i$, $i = 1, 3$, and the normal vectors $n_i = r_j \times r_k$ with $i \neq j \neq k$. Without loss of generality we require that $r_1 = s(r_2 \times r_3)$, so that r_1 is always normal to the level surfaces of action potential activity. The vectors r_2 and r_3 are tangent to the moving level surface. The scale factor s will be specified later.

We can calculate the entries α_{ij} explicitly. It follows from Cramer's rule that

$$\alpha_{ij} = \frac{(n_j)_i}{r_j \cdot n_j}, \quad \text{(no summation)} \tag{4.3}$$

where by $(n_j)_i$ we mean the ith component of the jth vector n_j.

Now we can write out the full change of variables. We calculate that

$$\begin{aligned} &\text{a)} \quad \frac{\partial \phi}{\partial t} = \frac{\partial \phi}{\partial \tau} - \frac{\partial X_j}{\partial \tau}\alpha_{jk}\frac{\partial \phi}{\partial \xi_k} \\ &\text{b)} \quad \frac{\partial}{\partial x_i}\left(d_{ij}\frac{\partial \phi}{\partial x_j}\right) = d_{ij}\alpha_{jp}\alpha_{ik}\frac{\partial^2 \phi}{\partial \xi_p\, \partial \xi_k} + \left(\frac{\partial d_{ij}}{\partial x_i}\alpha_{jp} + d_{ij}\alpha_{ik}\frac{\partial \alpha_{jp}}{\partial \xi_k}\right)\frac{\partial \phi}{\partial \xi_p}, \end{aligned} \tag{4.4}$$

so that equation (4.1) takes the form

$$\frac{\partial \phi}{\partial \tau} = d_{ij}\alpha_{jp}\alpha_{ik}\frac{\partial^2 \phi}{\partial \xi_p\, \partial \xi_k} + \left(\frac{\partial d_{ij}}{\partial x_i}\alpha_{jp} + d_{ij}\alpha_{ik}\frac{\partial \alpha_{jp}}{\partial \xi_k} + \frac{\partial X_j}{\partial \tau}\alpha_{jp}\right)\frac{\partial \phi}{\partial \xi_p} + f. \tag{4.5}$$

Our goal is to pick the new coordinate system so that the solution ϕ is a function of only one variable ξ_1. If this is done, then (4.5) reduces to

$$0 = d_{ij}\alpha_{j1}\alpha_{i1}\frac{\partial^2 \phi}{\partial \xi_1^2} + \left(\frac{\partial d_{ij}}{\partial x_i}\alpha_{j1} + d_{ij}\alpha_{ik}\frac{\partial \alpha_{j1}}{\partial \xi_k} + \frac{\partial X_j}{\partial \tau}\alpha_{j1}\right)\frac{\partial \phi}{\partial \xi_1} + f. \tag{4.6}$$

Now the equation (4.6) can be put into the form of (2.7) if we set

$$\begin{aligned} &\text{a)} \quad d_{ij}\alpha_{j1}\alpha_{i1} = 1 \\ &\text{b)} \quad \frac{\partial d_{ij}}{\partial x_i}\alpha_{j1} + d_{ij}\alpha_{ik}\frac{\partial \alpha_{j1}}{\partial \xi_k} + \frac{\partial X_j}{\partial \tau}\alpha_{j1} = c_0. \end{aligned} \tag{4.7}$$

These two requirements overdetermine the coordinate transformation $X(\xi, \tau)$, so we assume that the medium and the action potential front are slowly varying in space, and then interpret (4.7b) as determining the motion of the midline of the coordinate system, at the location of largest gradient of the action potential front.

Equation (4.7b), subject to the condition (4.7a) is the equation we seek to describe the motion of an action potential front. However, the interpretation of this equation is not obvious. We can get some further insight into the geometrical meaning of this equation by rewriting (4.7) making use of (4.3). We denote the propagating mid-surface by $R(\xi_2, \xi_3, \tau) = X(0, \xi_2, \xi_3, \tau)$ and find that

$$\frac{R_\tau \cdot r_1}{r_1 \cdot r_1} = c_0 - \frac{\partial d_{ij}}{\partial x_i}\frac{(r_1)_j}{r_1 \cdot r_1} - d_{ij}\sum_{k=1}^{3}\frac{(n_k)_i}{r_k \cdot n_k}\frac{\partial}{\partial \xi_k}\left(\frac{(r_1)_j}{r_1 \cdot r_1}\right). \tag{4.8}$$

It follows from differentiation of the normalization condition (4.7a) with respect to ξ_1, and symmetry of the coupling matrix, that

$$d_{ij}\alpha_{i1}\frac{\partial \alpha_{j1}}{\partial \xi_1} = -\tfrac{1}{2}r_1 \cdot \operatorname{grad}(d_{ij})\alpha_{i1}\alpha_{ji}. \tag{4.9}$$

Consequently,

$$\frac{R_\tau \cdot r_1}{r_1 \cdot r_1} = c_0 - Gr - K, \tag{4.10}$$

where

$$Gr = \frac{\partial d_{ij}}{\partial x_i}\frac{(r_1)_j}{r_1 \cdot r_1} - \tfrac{1}{2}r_1 \cdot \operatorname{grad}(d_{ij})\frac{r_{1j}r_{1i}}{(r_1 \cdot r_1)^2},$$

$$K = d_{ij}\left(\frac{(n_2)_i}{r_2 \cdot n_2}\frac{\partial}{\partial \xi_2} + \frac{(n_3)_i}{r_3 \cdot n_3}\frac{\partial}{\partial \xi_3}\right)\left(\frac{(r_1)_j}{r_1 \cdot r_1}\right),$$

$$\frac{d_{ij}(r_1)_i(r_1)_j}{(r_1 \cdot r_1)^2} = 1,$$

with $r_1 = s(r_2 \times r_3)$.

The expressions Gr and K can now be given physical interpretations. The expression Gr is nontrivial only if the coupling coefficients d_{ij} are nonhomogeneous in space, so the term Gr represents the change in velocity of the action potential front due to spatial variations in coupling. A similar term was found in the one dimensional case in (3.18). The term K is related to the curvature of the surface R, suitably modified to account for anisotropy. In the special case that $d_{ij} = d\delta_{ij}$, the gradient term becomes

$$Gr = \tfrac{1}{2}r_1 \cdot \frac{\operatorname{grad}(d)}{d}, \tag{4.11}$$

and the curvature term K becomes

$$K = -r_1 \cdot \frac{r_{22}(r_3 \cdot r_3) - 2r_{32}(r_2 \cdot r_3) + r_{33}(r_2 \cdot r_2)}{(r_2 \cdot r_2)(r_3 \cdot r_3) - (r_2 \cdot r_3)^2} = -\sqrt{d}\kappa, \tag{4.12}$$

where κ is twice the mean curvature of the mid-surface [33]. (The expression r_{ij} denotes $r_{ij} = \partial^2 X/\partial\xi_i\,\partial\xi_j$.) If we denote N to be the unit normal vector of the propagating mid-surface, then in the special case that $d_{ij} = d\delta_{ij}$, the equation (4.10) becomes

$$R_\tau \cdot N = c_0\sqrt{d} - \tfrac{1}{2}N \cdot \operatorname{grad}(d) + d\kappa. \tag{4.13}$$

In the case of uniform d, the equation (4.13) is the usual eikonal-curvature equation and has been studied extensively [19, 25, 36, 37].

A full study of equation (4.10) in a three dimensional domain requires numerical simulation. With a direct numerical approach, one could discretize some initial surface and allow it to evolve according to a discretization of (4.10). The difficulty with this numerical method is that the distribution of grid points on the surface changes as a function of time, and redistribution of the grid will be necessary from time to time to keep the grid somewhat uniform. This is a complicated process at best.

A better method is to view the evolving surface as a level set of some function $u(x, t)$ defined in all of space and to follow the evolution of the function u on a fixed three dimensional grid, and then to contour the evolving level set of u. A third (closely related) method is to assume that there is a function of space U whose t level set (i.e., the surface $U(x) = t$) specifies the wavefront at time t. We will explore the second of these three methods.

Suppose there is a function of space and time $u(x, t)$ whose level sets are the moving wavefronts we seek. The function $u(x, t)$ is the inverse of the function $X(\xi, t)$. We perform the same change of variables as in (4.4), now expressing the equation using the function $u(x, t)$. Following the same steps as before, we find an equation of motion that is equivalent to (4.7), namely,

$$\begin{aligned} &\text{a)} \quad d_{ij}\alpha_{j1}\alpha_{i1} = 1, \\ &\text{b)} \quad \frac{\partial R_j}{\partial \tau}\alpha_{j1} + \frac{\partial}{\partial x_i}(d_{ij}\alpha_{j1}) = c_0, \end{aligned} \tag{4.14}$$

where $\alpha_{i1} = -s(\nabla u)_i$. If $u(x, t) = \text{constant}$ describes a level surface R that propagates according (4.14), then $u_t = -\nabla u \cdot R_\tau$. It follows that

$$\begin{aligned} &\text{a)} \quad u_t = \frac{1}{s}\left(c_0 + \frac{\partial}{\partial x_i}(d_{ij}s(\nabla u)_j)\right), \\ &\text{b)} \quad s^2 d_{ij}(\nabla u)_i(\nabla u)_j = 1. \end{aligned} \tag{4.15}$$

Boundary conditions for u are that $\nabla u \cdot N_B = 0$ at a boundary, where N_B is the normal to the boundary.

5 Plane waves

Before examining fully three dimensional solutions of the eikonal-curvature equation, it is helpful to look for solutions with simplified geometry. Suppose that the medium is a slab of some fixed height, with the epicardial surface at

$z = 0$, and the endocardial surface at $z = L$. We take the x and y coordinates of the medium to be infinite, with the x axis aligned with the cell long axis on the epicardial surface. We look for simplified solutions that are propagating in the same $x-y$ direction everywhere. That is, at any z level, the wavefront is a straight line whose orientation in the $x-y$ plane is independent of height z. In spite of the title of this section, these are not plane waves because the wavefront surface is not a plane, but has a curved cross-section. However, these wavefronts can be viewed as two rather than three dimensional waves. We shall furthermore assume that the medium is anisotropic, but homogeneous. By homogeneous, we mean that the coefficients D_i in (2.4b) and (2.6) are independent of space, although the angle of cell orientation θ depends on $z = x_3$.

We first look for invariant wavefront solutions, that is, solutions whose cross-sectional profile does not change with time. We suppose that the direction of propagation of the wavefront in the $x-y$ plane makes an angle ψ with the x axis. The $x-y$ components of the normal vector of the wavefront surface are then specified everywhere by the vector $(\cos\psi, \sin\psi)$. Because the wave surface is planar in the $x-y$ coordinate plane, it is natural to describe the wavefront in terms of the three coordinates $\xi = x\cos\psi + y\sin\psi$, $\eta = -y\sin\psi + x\cos\psi$, and z, and to realize that the solution we seek is independent of η. We define the position vector for the wave surface in the ξ, η, z coordinate system by

$$R = \begin{pmatrix} \xi(z) + ct \\ \eta \\ z \end{pmatrix}, \tag{5.1}$$

and it follows that

$$r_1 = s\begin{pmatrix} 1 \\ 0 \\ -\xi'(z) \end{pmatrix}, \quad r_2 = \begin{pmatrix} \xi'(z) \\ 0 \\ 1 \end{pmatrix}, \quad r_3 = \begin{pmatrix} 0 \\ 1 \\ 0 \end{pmatrix}, \quad \text{where } \xi'(z) = \frac{d\xi}{dz}. \tag{5.2}$$

When we write the governing equations (2.2), (2.6) in the ξ, η, z coordinate system, we can make the identification

$$d_{11} = D_1\cos^2(\theta(z) - \psi) + D_2\sin^2(\theta(z) - \psi), \qquad d_{33} = D_3, \tag{5.3}$$

and all other coupling coefficients are either zero are not needed.

When we apply the normalization condition $d_{ij}(r_1)_i(r_1)_j/(r_1 \cdot r_1)^2 = 1$ to determine s, we find that

$$\frac{r_1}{r_1 \cdot r_1} = \frac{1}{\sqrt{d_{11} + d_{33}\xi'^2}}\begin{pmatrix} 1 \\ 0 \\ -\xi' \end{pmatrix}. \tag{5.4}$$

Next we calculate that

$$\frac{R_t \cdot r_1}{r_1 \cdot r_1} = \frac{c}{\sqrt{d_{11} + d_{33}\xi'^2}}, \qquad Gr = \frac{1}{2}\frac{\xi'}{1+\xi'^2}\frac{d'_{11}}{\sqrt{d_{11} + d_{33}\xi'^2}}$$

$$K = \frac{d_{11}\xi'}{1+\xi'^2}\frac{\partial}{\partial z}\left(\frac{1}{\sqrt{d_{11} + d_{33}\xi'^2}}\right) + \frac{d_{33}}{1+\xi'^2}\frac{\partial}{\partial z}\left(\frac{-\xi'}{\sqrt{d_{11} + d_{33}\xi'^2}}\right). \tag{5.5}$$

Finally, we set $y = \xi'/\sqrt{d_{11}d_{33}}$, introduce the dimensionless length scale ζ through $z = L\zeta$, and the equation (4.10) becomes

$$y' + p\left((1+y^2) - \frac{c}{s_0}\sqrt{\frac{D_1}{d_{11}}}\right)(1+y^2) = 0, \qquad p = \frac{c_0 L}{\sqrt{d_{33}}}, \tag{5.6}$$

where $s_0 = c_0\sqrt{D_1}$ is the speed of plane wave propagation on the epicardial surface in the direction of the cell axis.

To find the shape of a steadily propagating wave we must solve the equation (5.6) subject to the boundary conditions $y = 0$ at $\zeta = 0, 1$. These boundary conditions come from the requirement that the action potential wavefront be orthogonal to both the epicardial and endocardial surfaces.

The equation (5.6) is a first order ordinary differential equation that must be solved subject to two boundary conditions, i.e., it is a nonlinear eigenvalue problem for the unknown parameter c. It is easy to show, using standard phase plane arguments, that for any fixed value p there is a value of the constant c for which a solution is obtained, and this eigenvalue and the corresponding solution y is unique.

We cannot solve (5.6) analytically, although it is straightforward to solve the equation using numerical integration and a shooting method. Because the slope of the function y depends in a monotone way on the parameter c, we simply guess a value for the parameter c, integrate the equation from $\zeta = 0$ to $\zeta = 1$ starting with $y = 0$ at $\zeta = 0$. If the value of y at $\zeta = 1$ is positive we adjust c downward, and if the value of y at $\zeta = 1$ is negative we adjust c upwards, until a satisfactory estimate of the parameter c is found.

Specific parameter values can be chosen to represent typical myocardium. We take $D_3 = D_2 = D_1/9$, so that the speed of plane wave propagation on the epicardium is 3 times faster in the axial direction than in transverse directions, which is typical [35, 38]. We take $\theta(z) = 2\pi z/3L$, giving a counterclockwise rotation of the cell axis of 120 degrees from epicardial to endocardial surfaces. The only remaining parameter is the dimensionless parameter $p = c_0 L/\sqrt{d_{33}}$. With a speed of propagation of 50 cm/sec, a space constant along the fiber axis of 0.09 cm, a time unit of 7 msec, and wall thickness of 1 cm, we estimate $p = 130$.

In Fig. 1 is shown (solid curves) the speed of propagation, normalized so that the maximum possible speed is 1.0, as a function of the direction of propagation relative to the orientation of the fibers on the epicardial surface. Speeds are shown for the two parameter values $p = 1.0$ and $p = 5.0$. The dashed curves show the speed of propagation for thin epicardial and endocardial layers, without effects from tissue thickness. The epicardial speed is maximal at $\theta = 0$, when waves are aligned to propagate along epicardial fibers. Similarly, endocardial propagation speed is maximal at $\theta = 120$ degrees, when propagation is aligned with endocardial fibers.

The effect of increased p is to increase the speed of propagation. For large p, the equation (5.6) is stiff, and difficult to integrate numerically. However, one can find an asymptotic solution of the eigenvalue problem using singular perturbation methods and phase plane arguments.

When p is large (for example, $p = 130$ is large enough), to leading order in $1/p$, the eigenvalue c^* is

$$c^* = s_0 \max_{0 \le \theta \le \theta^*} \sqrt{\frac{d_{11}(\theta)}{D_1}}, \tag{5.7}$$

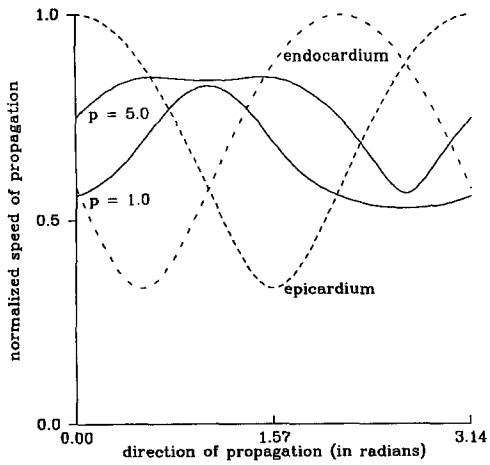

Fig. 1. Normalized speed of propagation plotted as a function of direction of propagation for parameter values $p = 1.0, 5.0$. Dashed curves show speed of propagation for epicardial and endocardial surfaces. For this plot, $D_2 = D_3 = D_1/9$

where the fiber orientation in the tissue varies between $\theta = 0$ and $\theta = \theta^*$. Recall that $d_{11}(\theta)$ is given by (5.3). In other words, the wavefront travels at the speed of the fibers with which it is most closely aligned. If ϕ^* is the value of θ at which the maximum is attained, then, everywhere except in a small boundary layer at $\zeta = 0$ and $\zeta = 1$, the wavefront profile y satisfies

$$\begin{aligned} &\text{a)} \quad y = \sqrt{\frac{c^*}{s_0}\sqrt{\frac{D_1}{d_{11}}} - 1}, \quad \text{if } \theta \leqslant \phi^*, \\ &\text{b)} \quad y = -\sqrt{\frac{c^*}{s_0}\sqrt{\frac{D_1}{d_{11}}} - 1}, \quad \text{if } \phi^* \leqslant \theta. \end{aligned} \tag{5.8}$$

Near $\zeta = 0$ and $\zeta = 1$, there are boundary layers that connect the "outer solution" (5.8) with $y = 0$.

We can now determine the speed of propagation as a function of direction of propagation ψ, in the limit that p is large. In the range $0 \leqslant \psi \leqslant \theta^*$, the function $d_{11}(\theta)$ has an interior maximum, so the speed of propagation is $c^* = s_0$. That is, the fibers that are best aligned with the wavefront determine the speed of the wavefront. In the range $\theta^* \leqslant \psi \leqslant (\theta^* + \pi)/2$, the function $d_{11}(\theta)$ has its maximum at $\theta = \theta^*$, so that the speed of propagation is determined by the endocardial surface to be $c^* = c_0\sqrt{D_1 \cos^2(\psi - \theta^*) + D_2 \sin^2(\psi - \theta^*)}$. Finally, in the range $(\theta^* + \pi)/2 \leqslant \psi \leqslant \pi$, the function $d_{11}(\theta)$ has its maximum at $\phi = \pi$, so the speed of propagation is $c^* = c_0\sqrt{D_1 \cos^2\psi + D_2 \sin^2\psi}$, determined by the epicardial surface. In summary, in the limit of large p (which is certainly a good approximation when $p = 130$)

$$\begin{aligned} &c^* = c_0\sqrt{D_1}, \quad 0 \leqslant \psi \leqslant \theta^*, \\ &c^* = c_0\sqrt{D_1 \cos^2(\psi - \theta^*) + D_2 \sin^2(\psi - \theta^*)}, \quad \theta^* \leqslant \psi \leqslant \frac{\theta^* + \pi}{2}, \\ &c^* = c_0\sqrt{D_1 \cos^2\psi + D_2 \sin^2\psi}, \quad \frac{\theta^* + \pi}{2} \leqslant \psi \leqslant \pi. \end{aligned} \tag{5.9}$$

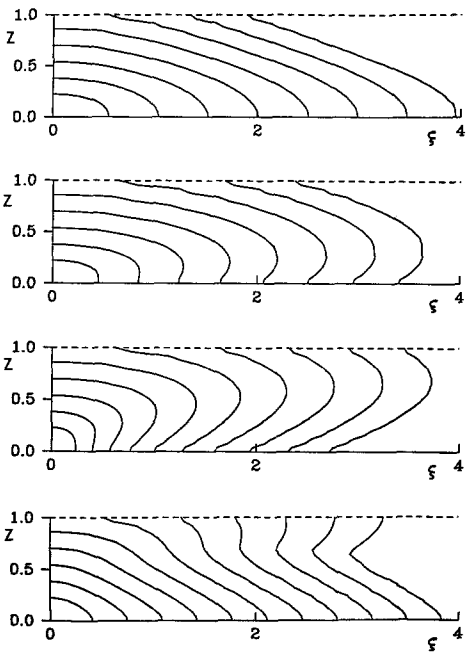

Fig. 2. Cross-sectional profiles of plane waves propagating in the directions $\psi = 0$, $\pi/4$, $\pi/2$, and $3\pi/4$ (top to bottom), initiated from the epicardial surface ($z = 0$), shown at 10 ms intervals. Parameters for this simulation were $D_1 = 0.0081$, $D_3 = 0.0009$, $c_0 = 3.89$, with a time unit $C_m R_m = 7$ ms. The vertical axis is z, with $z = 0$ corresponding to the epicardial surface, and $z = 1$ corresponding to the endocardial surface. The horizontal axis is the spatial coordinate ξ. Fibers were assumed to rotate through $2\pi/3$ from epicardium to endocardium. Spatial discretization was 0.04 cm on a 100×25 grid, corresponding to 4 cm × 1 cm cross-section of tissue

Further insight into the nature of this propagation is obtained by solving the eikonal-curvature equation numerically. The simplification to two dimensional waves implies that the eikonal-curvature equation has the simplified form

$$\begin{aligned} &\text{a)} \quad u_t = \frac{1}{s}\left(c_0 + d_{11}(z)\frac{\partial}{\partial \xi}\left(s\frac{\partial u}{\partial \xi}\right) + d_{33}\frac{\partial}{\partial z}\left(s\frac{\partial u}{\partial z}\right)\right) \\ &\text{b)} \quad s^2\left(d_{11}(z)\left(\frac{\partial u}{\partial \xi}\right)^2 + d_{33}\left(\frac{\partial u}{\partial z}\right)^2\right) = 1, \end{aligned} \tag{5.10}$$

where $d_{11}(z)$ is specified by (5.2).

In Fig. 2 are shown examples of how the planar wavefront evolves following an initial stimulus at the epicardial surface. Shown are cross-sectional profiles of the propagating wavefront at 10 ms time intervals, starting at time $t = 10$ ms, for propagation in the directions (top to bottom) $\psi = 0$, $\pi/4$, $\pi/2$, and $3\pi/4$. In these figures, the vertical axis is z, with $z = 0$ corresponding to the epicardium, and $z = 1$ corresponding to the endocardium, and the horizontal axis length ξ, in units of cm. For these simulations, we used a time constant of $C_m R_m = 7$ ms, a space constant in the direction of fibers $\sqrt{D_1} = 0.09$ cm. The velocity of propagation along the long axis of myocardial fibers is typically on the order of 0.5 m/sec, yielding $c_0 = 0.5 C_m R_m / \sqrt{D_1} = 3.89$. We also used $D_3 = D_2 = D_1/9$, to account for the fact that propagation transverse to fibers is about three times slower than along the fiber axis. The grid size was .04 cm on a 100×25 grid yielding a 4 cm × 1 cm domain. Total fiber rotation through the myocardium was taken as $2\pi/3$. The numerical discretization scheme was an explicit order h^2 Euler scheme. The slight oscillations seen in some of the profiles result from a boundary layer at the edges of the domain that is not adequately resolved by the uniform grid.

These figures show some noteworthy features. As predicted by (5.9), the speed of propagation for angles $\psi = 0$, $\pi/4$, and $\pi/2$ is determined by the speed of fibers with which the wavefront direction is most closely aligned, on the epicardium at $\psi = 0$, and in the midwall at $\psi = \pi/4$ and $\pi/2$. The speed of propagation for $\psi = 3\pi/4$ is ultimately determined by the endocardial surface, but only after more time and space than shown in Fig. 2 (bottom).

In all cases, propagation on the endocardial surface is initially much faster than predicted by propagation along endocardial fibers. This is obviously because the wavefront is nearly parallel to the endocardial surface at the time of first intersection, so the apparent endocardial surface velocity is greatly enhanced by the wavefront coming from within the wall. Similarly, when $\psi = \pi/4$, and $\pi/2$ (the middle two views in Fig. 2) activation can be viewed as coming from within the wall, even though the initial stimulus was applied at the epicardium. Thus, one could argue that the action potential which was initiated at the epicardium first traveled into the midwall where it accelerated along aligned fibers before reemerging onto the epicardium.

6 Waves in a three dimensional domain

In this section we discuss results of numerical simulation of the eikonal-curvature equation in the form (4.15) for a three dimensional domain. This equation with $d_{ij} = \delta_{ij}$ and $c_0 = 0$ has been used successfully to study evolution of a surface by its mean curvature [26, 30]. The advantage of the formulation (4.15) over the evolution equation (4.10) for numerical computations is that we seek a function u on a fixed three dimensional spatial grid and need not concern ourselves with the difficult problem of working with a moving, changing grid. However, this formulation also has some disadvantages. First, one must solve the equation on a three dimensional grid, rather than on a two dimensional surface, and the requisite computer space increases substantially, although the three dimensional grid needed for (4.15) is not nearly as large as would be necessary to simulate a full ionic current model. Second, there are many "wasted" computations, since only the zero level set is used, even though all level sets satisfy the same evolution equation, starting from different initial data. It is possible to streamline the computation to solve (4.15) only in a neighborhood of the zero level set of u.

A slightly different approach is used in [7] to solve the eikonal-curvature equation for two dimensional isotropic layers. There, the level surface $u(x, t) = 0$ is written as $u(x, t) = U(x) - t = 0$, and then (4.15) becomes a nonlinear equation for $U(x)$ on a three dimensional grid. This approach has the advantage that all of the contours of $U(x)$ have a physical interpretation, being the position of the wavefront at time t, but it has the disadvantage that the problem is nonlinear and therefore requires a time consuming and numerically sophisticated nonlinear interation procedure to obtain solutions, and it is harder to specify initial conditions.

The computations presented here were done using an explicit order (h^2) discretization of the equation (4.15), keeping in mind that for stability of the method, the temporal step size must be restricted to be of the order of h^2. A fully explicit method has the advantage that it consumes fewer manhours to set up at the cost of requiring more computer hours to calculate. The simulations discussed in this section typically used 10 cpu hours on a VAX 8600, but the code required only a few hours to write and debug. If more extensive simulations of

this equation are needed, a more sophisticated, implicit scheme will be preferred [26, 30].

For numerical computations, parameter values were estimated as in Section 5. We chose a time constant of $C_m R_m = 7$ ms, and a space constant in the direction of fibers $\sqrt{D_1} = 0.09$ cm. The velocity of propagation in normal myocardium along the long axis of fibers is about 0.5 m/sec, yielding $c_0 = 3.89$. We also chose $D_3 = D_2 = D_1/9$, to account for the fact that propagation transverse to fibers is about three times slower than along the fiber axis. For a three dimensional domain the coupling coefficients are

$$\begin{aligned} d_{11}(z) &= D_1 \cos^2 \theta(z) + D_2 \sin^2 \theta(z), \\ d_{12}(z) &= d_{21}(z) = (D_1 - D_2) \sin \theta(z) \cos \theta(z), \\ d_{22}(z) &= D_1 \sin^2 \theta(z) + D_2 \cos^2 \theta(z), \end{aligned} \tag{6.1}$$

with $d_{33} = D_3$.

To study the wavefronts that emanate from a point stimulus, two numerical experiments using the eikonal-curvature equation were performed. In the first we simulated the equation on a $100 \times 100 \times 20$ grid of points with spatial discretization 0.05 cm, corresponding to a piece of tissue 5 cm $\times$ 5 cm $\times$ 1 cm having total fiber rotation of 120 degrees. Initial data were a small spherical wavefront of radius 0.15 cm centered at about 0.46 cm depth. The equations were integrated for 50 ms of physical time.

In Figs. 3a, b, c, d, and e are the profiles of the wavefront at different depths in the tissue at 10 ms intervals ending at 50 ms. In each of the figures, the dashed lines indicate fiber orientation. Not all of the figures show five isochrons because at early times the wavefront does not intersect all level surfaces. There are a number of striking features of these figures. Perhaps the most obvious is that none of the oblong spreading wavefront shapes is in exact alignment with the fiber orientation at that level. At $z = 0.0$ cm, the oblong shapes are about 25 degrees out of alignment, and at $z = 1.0$ cm they are also about 25 degrees out of alignment, but in the opposite direction. Of necessity there is one level surface somewhere in the midwall region at which the alignment is exact, but for this simulation, exact alignment is not at $z = 0.5$ cm. The oblong shapes rotate through about 65 degrees while the fiber orientation rotates through 120 degrees.

The second striking feature is that the wavefront shapes can be described as oblong, roughly elliptical, but there are significant departures from strict ellipticity. In the outer layers, the shapes are fatter than ellipses, and they are not symmetric with respect to their major axis. There is a slight thickening of the shape at $z = 0.0$ cm in the counterclockwise direction due to the influence of the wavefront deeper within the tissue. This effect can be clearly seen by overlaying Figs. 3a and 3b. The second interesting variation from strict ellipticity is in the interior layers, where there is a noticeable "dimpling" of the waveshapes. This can again be traced to the effect of neighboring layers.

For propagation in three dimensional tissue, care must be taken with the definition of propagation velocity. If we measure propagation velocity simply (or naively) as the distance between measuring sites divided by the time of travel between the measuring sites, we will obtain artificially high apparent velocities. This can be seen by using a ruler on Figs. 3a–e. One can measure that the separation between curves in Fig. 3c corresponds to about 0.49 m/sec in the long

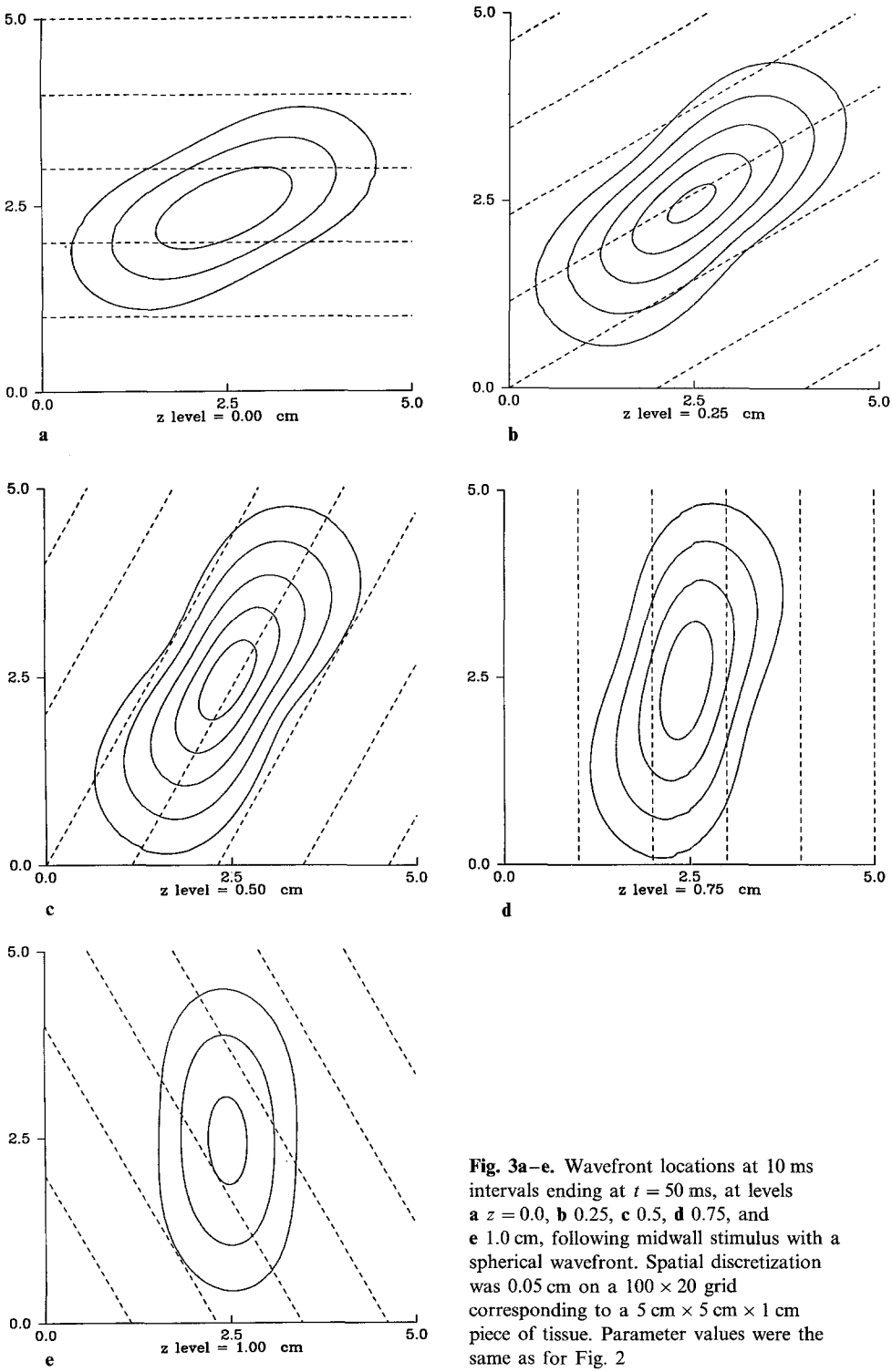

Fig. 3a–e. Wavefront locations at 10 ms intervals ending at $t = 50$ ms, at levels **a** $z = 0.0$, **b** 0.25, **c** 0.5, **d** 0.75, and **e** 1.0 cm, following midwall stimulus with a spherical wavefront. Spatial discretization was 0.05 cm on a 100×20 grid corresponding to a 5 cm $\times$ 5 cm $\times$ 1 cm piece of tissue. Parameter values were the same as for Fig. 2

axis direction and 0.18 m/sec in the short axis direction. This is slightly smaller than expected (0.5 m/sec) in the long direction and slightly larger than expected (0.17 m/sec) in the short direction because of curvature effects. It is not hard to recognize that at $z = 0.0$ cm (Fig. 3a) velocities are larger than 0.5 m/sec. In fact in the time interval from 20 ms to 30 ms the average apparent velocity is in excess of 1 m/sec.

Of course, this large apparent velocity is an artifact of the way velocity is measured. Whenever velocity is measured as the rate of movement of the intersection of one moving surface with another fixed surface, the velocities can be made as high as you wish by picking the measuring surface to be nearly parallel to the moving surface. The preferred definition of velocity is the normal velocity of the moving wave surface. At $z = 0.5$ cm, the wavefront is nearly vertical with respect to the z level surface and so velocity measurement in the $z = 0.5$ cm plane gives an accurate measure of the normal velocity. At $z = 0.0$ cm, however, the wavefront is nearly parallel to the level surface at early times and therefore registers artifactually high apparent velocities. The normal velocity never exceeds the expected values of 0.5 m/sec.

The second numerical experiment was to simulate the eikonal-curvature equation using initial data corresponding to a small hemispherical initial wavefront of radius 0.15 cm applied at the epicardial surface. This simulation was performed on a $120 \times 120 \times 15$ grid with spatial discretization 0.05 cm, corresponding to a piece of tissue 6 cm $\times$ 6 cm $\times$ 0.75 cm, having total fiber rotation of 90 degrees. In Figs. 4a, b, c, and d are shown the shapes of the wavefronts at different z levels at 10 ms intervals ($t = 10$–60 ms in 4a, 20–60 ms in 4b, 30–70 ms in 4c, and 50–70 ms in 4d).

There are some striking features seen in these figures. Most obvious is again that the long axis of the expanding oblong shapes is not in the direction of the fiber orientation. On the epicardial surface, the long axis of expansion is about 5 degrees from the fiber direction and on the endocardial surface is about 30 degrees from the fiber direction. There is roughly 55 degrees of rotation of the oblong expanding shapes with 90 degrees of fiber rotation.

There are substantial differences between the shapes on the epicardial and endocardial surfaces. On the epicardium, the oblong shapes are rather close to being three times longer than wide. There is noticeable dimpling, bulging and counterclockwise rotation due to the effects of underlying layers. On the endocardial surface, the ellipticity is much less pronounced, being in a ratio of roughly 3 to 2.

Once again, the preferred definition of velocity of propagation is the velocity in the direction of the normal to the propagating wavefront. Using this definition, we can discuss the path of travel of a piece of the wavefront by viewing activation as traveling along the normal to the wavefront surface. The collection of normal vectors for the wavefront at different times gives a vector field over all of space defining the direction of action potential travel. Individual paths of travel are defined as integral curves of the normal vector field.

The rotation of fibers now gives an interesting twist to the paths of travel. On the epicardial surface, there is noticeable bulging of the elliptical shapes in the direction of fiber rotation. This results from a path of travel that at first burrows down into the midwall region where it travels faster than it could have on the epicardial surface, then emerging again at some accelerated position on the epicardial surface. Thus, propagation into and out of the midwall allows for faster time of travel than propagation along the epicardium.

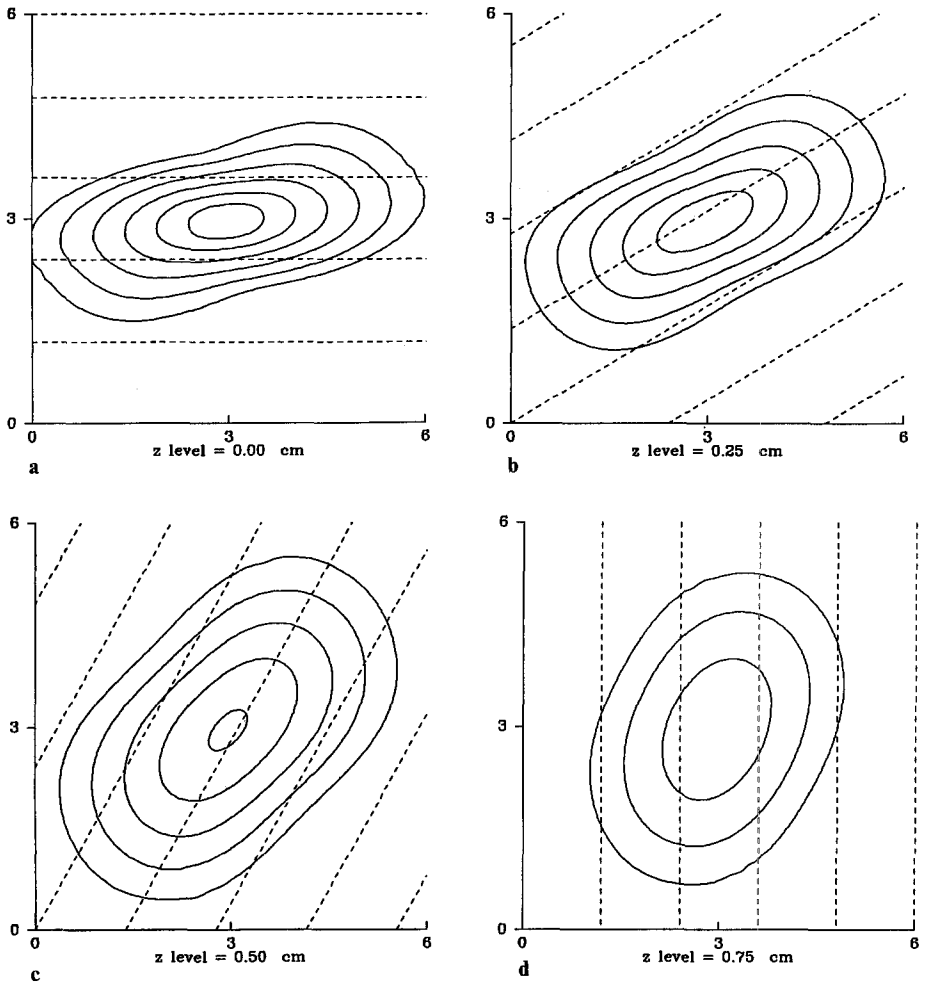

Fig. 4a–d. Wavefront locations at 10 ms intervals **a** $t = 10$–60 ms, **b** $t = 20$–60 ms, **c** $t = 30$–70 ms, **d** $t = 50$–70 ms at levels $z = 0.0$, 0.25, 0.5, and 0.75 cm, following epicardial stimulus with a hemispherical wavefront. Spatial discretization was 0.05 cm on a 120 × 120 × 15 grid corresponding to a 6 cm × 6 cm × 0.75 cm piece of tissue. Parameter values were the same as for Fig. 2.

7 Discussion

The results of this study show that rotating fiber orientation is important in determining the shape of action potential wavefronts. These results show that changing fiber orientation can be responsible for deforming wavefronts from the strictly elliptical shapes that are commonly observed in mapping studies of thin layers of myocardial tissue. Furthermore, in three dimensional tissue, the long axis of spreading oblong shapes is not expected to be aligned with fiber orientation.

The results of this study are consistent with available experimental data. However, some of these results have not yet been confirmed experimentally,

partly because three dimensional measurements have not yet been carried out with the same resolution as these numerical simulations. Principal among the unconfirmed results are the variation of cross-sectional profile of plane waves as a function direction of propagation, and the apparent acceleration of epicardial action potential propagation due to "tunneling" into the midwall.

This study makes essential use of the eikonal-curvature equation. In fact, with standard ionic models rather than the eikonal-curvature equation a study for three dimensional tissue patches of the size used here is computationally impossible. Furthermore, some aspects of the eikonal-curvature equation can be understood by purely analytical means.

References

1. Aronson, D. G., Weinberger, H. F.: Nonlinear diffusion in population genetics, combustion and nerve pulse propagation. In: Goldstein, J. A. (ed.) Partial Differential Equations and Related Topics. Berlin Heidelberg New York: Springer 1975
2. Balke, C. W., Lesh, M. D., Spear, J. F., Kadish, A., Levine, J. H., Moore, E. N.: Effects of cellular uncoupling on conduction in anisotropic canine ventricular myocardium. Circ. Res. **63**, 879–892 (1988)
3. Beeler, G. W., Reuter, H.: Reconstruction of the action potential of myocardial fibers. J. Physiol. (London) **268**, 177–210 (1977)
4. Burton, W. K., Cabrera, N., Frank, F. C.: The growth of crystals and the equilibrium structure of their surfaces. Phil. Trans. Roy. Soc. Lond. A **243**, 299–358 (1951)
5. Cole, J. D.: Perturbation Methods in Applied Mathemetics. Waltham, Ma.: Blaisdel 1968
6. Cole, W. C., Picone, J. B., Sperelakis, N.: Gap junction uncoupling and discontinuous propagation in the heart. Biophys. J. **53**, 809–818 (1988)
7. Colli-Franzone, P., Guerri, L., Rovida, S.: Wavefront propagation in an activation model of the anisotropic cardiac tissue: Asymptotic analysis and numerical simulations. J. Math. Biol. **28**, 121–176 (1990)
8. Delgado, C., Steinhaus, B., Delmar, M., Chialvo, D. R., Jalife, J.: Directional differences in excitability and margin of safety for propagation in sheep ventricular epicardial muscle. Circ. Res. **67**, 97–110 (1990)
9. Diaz, P. J., Rudy, Y., Plonsey, R.: Intercalated discs as a cause for discontinuous propagation in cardiac muscle: A theoretical simulation. Ann. Biomed. Eng. **11**, 177–189 (1983)
10. Ebihara, L., Johnson, E. A.: Fast sodium current in cardiac muscle, a quantitative description. Biophys. J. **32**, 779–790 (1980)
11. Fife, P. C.: Mathematical Aspects of Reacting and Diffusing Systems. (Lect. Notes Biomath.) Berlin Heidelberg New York: Springer 1979
12. Foerster, P., Muller, S. C., Hess, B.: Curvature and propagation velocity of chemical waves. Science **241**, 685–687 (1988)
13. Frankel, M. L., Sivashinsky, G. I.: On the equation of a curved flame front. Physica D **30**, 28–42 (1988)
14. Frazier, D. W., Krassowska, W., Chen, P. S., Wolf, P. D., Danieley, N. D., Smith, W. M., Ideker, R. E.: Transmural activations and stimulus potentials in three-dimensional anisotropic canine myocardium. Circ. Res. **63**, 135–146 (1988)
15. Hodgkin, A. L., Huxley, A. F.: A quantitative description of membrane current and its application to conduction and excitation in nerve. J. Physiol. **177**, 500–544 (1952)
16. Joyner, R. W.: Effects of the discrete pattern of electrical coupling on propagation through an electrical syncytium. Circ. Res. **50**, 192–200 (1982)
17. Joyner, R. W., Veenstra, R., Rawling, D., Chorro, A.: Propagation through electrically coupled cells; effects of a resistive barrier. Biophys. J. **45**, 1017–1025 (1984)
18. Kawato, M., Yamanaka, A., Urushiba, S., Nagata, O., Irisawa, H., Suzuki, R.: Simulation analysis of excitation conduction in the heart: Propagation of excitation in different tissues. J. Theor. Biol. **120**, 389–409 (1986)

19. Keener, J. P.: A geometrical theory for spiral waves in excitable media. SIAM J. Appl. Math. **46**, 1039–1056 (1986)
20. Keener, J. P.: Principles of Applied Mathematics: Transformation and Approximation. Reading, Ma.: Addison-Wesley 1988
21. Keener, J. P.: The effects of discrete gap junction coupling on propagation in myocardium. J. Theor. Biol. **148**, 49–82 (1991)
22. McAllister, R. E., Noble, D., Tsien, R. W.: Reconstruction of the electrical activity of cardiac Purkinje fibers. J. Physiol. **251**, 1–59 (1975)
23. Nielson, P. M. F., LeGrice, I. J., Smalil, B. H., Hunter, P. J.: Mathematical model of geometry and fibrous structure of the heart. Am. J. Physiol. **260**, H1365–H1378 (1991)
24. Noble, D., Noble, S. J.: A model of sino-atrial node electrical activity based on a modification of the DiFrancesco–Noble (1984) equations. Proc. Roy. Soc. Lond. **B222**, 295–304 (1984)
25. Ohta, T., Mimura, M., Kobayashi, R.: Higher-dimensional localized patterns in excitable media. Physica D **34**, 115–144 (1989)
26. Osher, S., Sethian, J. A.: Fronts propagating with curvature-dependent speed: Algorithms based on Hamilton–Jacobi formulations. J. Comp. Phys. **79**, 12–49 (1988)
27. Plonsey, R.: The use of a bidomain model for the study of excitable media. In: Othmer H. G. (ed.) Some Mathematical Questions in Biology. Providence: AMS 1989
28. Roberge, F. A., Vinet, A., Victorri, B.: Reconstruction of propagated electrical activity with a two-dimensional model of anisotropic heart muscle. Circ. Res. **58**, 461–475 (1986)
29. Rudy, Y., Quan, W.-L.: A model study of the effects of the discrete cellular structure on electrical propagation on cardiac tissue. Circ. Res. **61**, 815–823 (1987)
30. Sethian, J. A.: Numerical algorithms for propagating interfaces: Hamilton–Jacobi equations and conservation laws. J. Differ. Geom. **31**, 131–161 (1990)
31. Spach, M. S., Kootsey, J. M.: The nature of electrical propagation in cardiac muscle. Am. J. Physiol **244**, H3–H22 (1983)
32. Spach, M. S., Miller, W. T., Geselowitz, D. B., Barr, R. C., Kootsey, J. M., Johson, E. A.: The discontinuous nature of propagation in normal canine cardiac muscle. Circ. Res. **48**, 39–54 (1981)
33. Stoker, J. J.: Differential Geometry. New York: Wiley-Interscience 1969
34. Streeter, D. D.: Gross morphology and fiber geometry of the heart. In: Berne, R. M., Sperelakis, N., Geigert, S. R. (eds.) Handbook of Physiology. Baltimore: Williams and Wilkins 1979
35. Tsuboi, N., Kodama, I., Toyama, J., Yamada, K.: Anisotropic conduction properties of canine ventricular myocardium, influence of high extracellular K^+ concentration and stimulation frequency. Jap. Circ. J. **49**, 487–498 (1985)
36. Tyson, J. J., Keener, J. P.: Spiral waves in a model of myocardium. Physica D **29**, 215–222 (1987)
37. Tyson, J. J., Keener, J. P.: Singular perturbation theory of traveling waves in excitable media (a review). Physica D **32**, 327–361 (1988)
38. Wiedmann, S.: Electrical constants of trabecular muscle on mammalian heart. J. Physiol. (London) **118**, 348–360 (1970)
39. Yanagihara, K., Noma, A., Irisawa, H.: Reconstruction of sino-atrial node pacemaker potential based on the voltage clamp experiments. Jpn. J. Physiol. **30**, 841–857 (1980)